New Journal of Physics
The open access journal at the forefront of physics

Deutsche Physikalische Gesellschaft DPG
IOP Institute of Physics

Published in partnership with: Deutsche Physikalische Gesellschaft and the Institute of Physics

OPEN ACCESS

RECEIVED
29 August 2017

REVISED
6 February 2018

ACCEPTED FOR PUBLICATION
7 February 2018

PUBLISHED
5 March 2018

PAPER

Quantum state and mode profile tomography by the overlap

J Tiedau[1], V S Shchesnovich[2], D Mogilevtsev[2,3], V Ansari[1], G Harder[1], T J Bartley[1], N Korolkova[4] and Ch Silberhorn[1]

[1] Applied Physics, University of Paderborn, Warburgerstrasse 100, D-33098 Paderborn, Germany
[2] Centro de Ciencias Naturais e Humanas, Universidade Federal do ABC, Santo Andre, SP, 09210-170 Brazil
[3] Institute of Physics, Belarus National Academy of Sciences, F.Skarina Ave. 68, Minsk 220072 Belarus
[4] School of Physics and Astronomy, University of St Andrews, North Haugh, St Andrews KY16 9SS, United Kingdom

E-mail: johannes.tiedau@uni-paderborn.de

Keywords: quantum optics, photon statistics, tomography, quantum state tomography, homodyne detection

Abstract

Any measurement scheme involving interference of quantum states of the electromagnetic field necessarily mixes information about the spatiotemporal structure of these fields and quantum states in the recorded data. We show that in this case, a trade-off is possible between extracting information about the quantum states and the structure of the underlying fields, with the modal overlap being either a goal or a convenient tool of the reconstruction. We show that varying quantum states in a controlled way allows one to infer temporal profiles of modes. Vice versa, for the known quantum state of the probe and controlled variable overlap, one can infer the quantum state of the signal. We demonstrate this trade-off by performing an experiment using the simplest on–off detection in an unbalanced weak homodyning scheme. For the single-mode case, we demonstrate experimentally inference of the overlap and a few-photon signal state. Moreover, we show theoretically that the same single-detector scheme is sufficient even for arbitrary multi-mode fields.

1. Introduction

Quantum optical technologies are built on the generation, manipulation and detection of quantum states in well-defined modes of the electromagnetic field. Quantum state tomography (QST) [1, 2] describes the identification and reconstruction of quantum states, and is therefore an essential tool with both fundamental and practical applications. Optical QST can be performed using a variety of different methods; common to each is the variation of a known probe field which interferes with a signal, followed by extraction of information about the signal from the resulting measurement. In standard homodyne tomography, the bright probe (local oscillator—LO) field acts as an optical amplifier and mode filter. Scanning phase space by varying the LO phase, balanced homodyne detection then facilitates measurement of the quasi probability distribution, fully characterizing the quantum state. Successful reconstruction of the state requires high mode overlap between the signal and the LO, since any mode mismatch manifests as loss and is highly detrimental to the scheme [1, 2]. In weak-field homodyne detection, the LO is replaced by a coherent probe field of mean intensity comparable to the signal, typically of the order $|\alpha|^2 \sim 1$. Here, the magnitude as well as the phase of the weak probe is varied and the state may be reconstructed from the photon-counting statistics following interference of the two beams [3]. In contrast to strong-field homodyning, part of the signal which does not interfere with the weak probe is still detected, such that additional information about the state may be obtained. For particular interaction parameters, an elegant interpretation of the weak-field approach is the direct probing of the Wigner function by sampling phase space at a point determined by the amplitude and phase of the probe [4]. Not only coherent probes and interactions can be used to reconstruct the photon number distribution of a signal state, noise and losses can also be exploited for this purpose [5–9]. For example, in noise tomography varying the amplitude of probe in thermal state and a single on–off detector are sufficient [6] for quantum state diagnostics.

In this Paper, we present a method for state tomography based on imperfect and variable overlap of the signal and probe in unbalanced homodyning scheme. Crucially, our method also allows to extract information

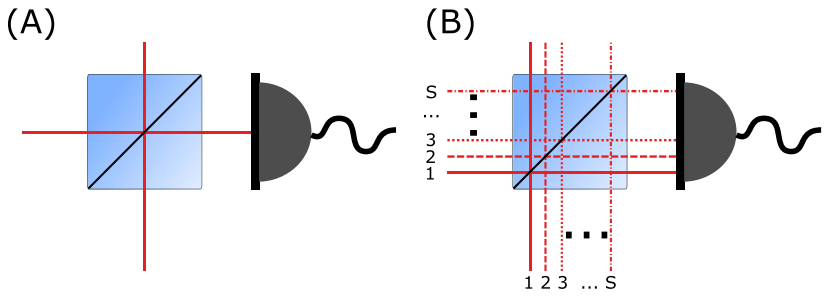

Figure 1. (A) A scheme of the simplest measurement set-up. Two incoming modes (signal and probe) are combined on a beam splitter. One outgoing mode from the beam splitter is measured with an on/off detector. (B) A general scheme of the weak-probe measurement set-up for multi-mode signal and probe fields. Two sets of S incoming modes (signal and probe) are combined on a beam splitter. A set outgoing from one of the beam splitter outputs is measured with an on/off detector.

about the underlying mode structure. Indeed, given a known quantum state occupying an unknown mode, this method can be used to infer the overlap, and, thus, to identify the shape of this mode. In this sense, it may be considered as a diagnostic tool for existing tomographic reconstructions schemes, where identifying the modes is crucial to measuring the whole state [10]. Several techniques have been shown to shape temporal mode profiles [11–18, 30–35] and the method to infer a modal temporal profile has a considerable practical value.

We demonstrate these techniques experimentally using heralded single and two-photon states in well-defined modes and coherent probe field. The suggested tomographic scheme is resource efficient, requiring a single on–off detector. We show that for an arbitrary known signal with a diagonal density matrix, the overlap modulus can be found from just one measurement. This can be an important advantage over, for example, standard quantum homodyne tomography with a strong probe. For instance, for single-photon strong-probe homodyning, involved algorithms for fitting the temporal profile are needed for reconstruction [19]. Moreover, by weak-probe homodyning it is possible to infer the overlap even for the unknown quantum state of the signal [9]. For that, measurements should be done for the set of different detection efficiencies, in addition to the variation in a controlled way of the quantum state of the probe. Note that the variable overlap can be also used for the reconstruction with the thermal probe. Finally, theoretically, we extend the scheme to cover the more general case where the signal occupies multiple modes.

The outline of the paper is as follows. In section 2 we introduce the concept of the overlap and temporal profile, describe the scheme and discuss the role of the overlap for the simplest single-mode case. In section 3 we describe the measurement set-up and experimental results for the signal state reconstruction for single-photon and two-photon signals. We also discuss there the inference of the overlap and give the experimental illustration for the single-photon state. In section 4 we describe the extension of our scheme for the multi-mode case.

In section 2, appendix B and at the end of the experimental section 3 we explicitly address the specific features and advantages of harnessing the imperfect overlap in weak-probe scheme for reconstruction. We show that the temporal profile of the signal can be found from a set of overlap values obtained by the simple time-delay of the probe pulse, for different profiles of the probe. For our weak-probe scheme, the overlap modification by the time-delay of the probe pulse also gives a sufficient degree of control for building a set of measurements for the reconstruction of the signal state. We show that varying the overlap is not equivalent to varying the probe field amplitude, and in some cases variation of the overlap provides an informational advantage over weak-field homodyne tomography. Using the Fisher information parameter [20], we have shown that for our scheme variation of the overlap can be significantly more efficient than variation of the amplitude of the probe state.

2. The scheme and the trade-off for the single-mode case

To demonstrate the basic features of the reconstruction of modal profiles and quantum states and trade-off between them, let us consider the simplest interference-based measurement scheme consisting of just one beam-splitter (BS) and on/off detector depicted in figure 1(A). The signal pulse interferes on the BS with the probe pulse of a comparable intensity, the result is impinging on the detector, and the number of clicks is recorded. Let us start our consideration with the simplest single-mode case.

For illustration, we start with a methodologically and practically important case of the probe and signal fields in single-mode spectrally pure states. We assume that the input temporal modes of the same polarization in figure 1(A) are described by the collective operators

$$A_x = \int_0^\infty \mathrm{d}\omega f_x(\omega) a_x(\omega), \tag{1}$$

where the index x denotes either signal, s, or probe, p, modes; $_{ax}(w)$ is the annihilation operator of the photon in the plane wave with the frequency ω; $\int_0^\infty \mathrm{d}\omega |f_x(\omega)|^2 = 1$. Again, we assume that both inputs are single mode and in the same spatial mode. Thus, a degree of distinguishabity is described by the overlap

$$\phi_1 = \int_0^\infty \mathrm{d}\omega f_s(\omega) f_p(\omega)^*. \tag{2}$$

We assume that the BS acts similarly on input plane wave modes of arbitrary frequency.

For the BS with the transmittivity T, the probability to register 'no click' on the detector is given by the following equation [4]:

$$p = \mathrm{Tr}\{:\exp\{-T^2\eta(a_s^\dagger a_s + \mu^2 a_p^\dagger a_p + \mu\phi_1 a_s^\dagger a_p + \mu\phi_1^* a_p^\dagger a_s)\}: \rho_p \rho_s\}, \tag{3}$$

where :: denotes the normal ordering operator, η is the detection efficiency, and $\mu = \sqrt{(1-T)/T}$. Initial states are described by the density matrices ρ_x. Equation (3) gives a picture of the influence of distinguishability on the measurement result. For the low overlap, $|\phi_1| \ll 1$, the probability is close to the product of two 'no click' probabilities for the signal and probe states. For $|\phi_1| \to 1$, the detector is measuring a single superposition mode. Equation (3) gives also a clear hint about additional possibilities given by the overlap control: for example, changing a respective overlap phase by π is equivalent to measuring the outcome of the other port of a balanced BS.

To get more insight, let us represent both the signal and the probe as the sum of the coherent projectors

$$\rho_{s(p)} = \sum_j c_j^{s(p)} |\alpha(\beta)_j\rangle \langle \alpha(\beta)_j|, \tag{4}$$

where the coefficients $c_j^{s(p)}$ are real, but not necessarily positive. A finite discrete representation of this kind is usually implemented in data-pattern tomography schemes [21–25]. From equation (3) we get

$$p = \sum_{jk} c_j^s c_k^p \exp\{-T^2\eta(|\alpha_j|^2 + \mu^2|\beta_k|^2 + \mu\phi_1\alpha_j^*\beta_k + \mu\phi_1^*\beta_k^*\alpha_j)\}. \tag{5}$$

From equation (5) shows both the possibility to infer the overlap, ϕ_1, for the known signal by fitting the registered signal with the model one for different probes, and to build a set of measurements sufficient for inferring a signal state by controlled change of the overlap.

2.1. Inferring the overlap

Let us prove that it is indeed possible to infer the overlap between an arbitrary known signal state and the known probe by varying the probe state. First of all, let us assume that the probe is in the coherent state, $|\beta\rangle$, and re-write equation (5) for the case as

$$p = \langle\bar{\beta}|\bar{\rho}_s|\bar{\beta}\rangle \exp\{-(1-T^2)\eta|\beta|^2(1-|\phi_1|^2)\}, \tag{6}$$

where the matrix $\bar{\rho}_s$ is the density matrix of the damped signal, i.e., transformed in the following way

$$\rho_s = \sum_j c_j^s |\alpha_j\rangle\langle\alpha_j| \to \bar{\rho}_s = \sum_j c_j^s |\sqrt{\eta}\,T\alpha_j\rangle\langle\sqrt{\eta}\,T\alpha_j|, \tag{7}$$

and the damped amplitude of the probe is $\bar{\beta} = -\sqrt{\eta(1-T^2)}\,\phi_1^*\beta$.

Now let us measure the zero-click probability, p, for the randomly and homogeneously varying phase of the probe field. After averaging over the random phase, we obtain the following formula

$$p = \sum_{n=0}^\infty f_n \frac{\eta^n|\phi_1\beta|^{2n}(1-T^2)^n}{n!} \exp\{-(1-T^2)\eta|\beta|^2\}, \tag{8}$$

where f_n are diagonal elements of the damped signal density matrix $\bar{\rho}_s$ in the Fock-state basis. A remarkable property of equation (8) is the monotonous dependence of the probability p on the modulus of the overlap, $|\phi_1|$. So, a measurement with just one randomized-phase probe is sufficient to infer the modulus of the overlap for an arbitrary signal state. Obviously, for the known diagonal signal just one probe is sufficient for inferring the modulus of the overlap. After inferring the modulus of the overlap, one can easily fit the phase taking a measurement for the probe with a particular phase. The illustration of the overlap inference is shown in figure 2. The dependence of the zero-click probability on the overlap modulus for the phase-averaged probe is shown in figure 2(a) for the coherent and single-photon signal. Panels figures 2(b), (c) illustrate an influence of the relative overlap phase on the zero-click probability.

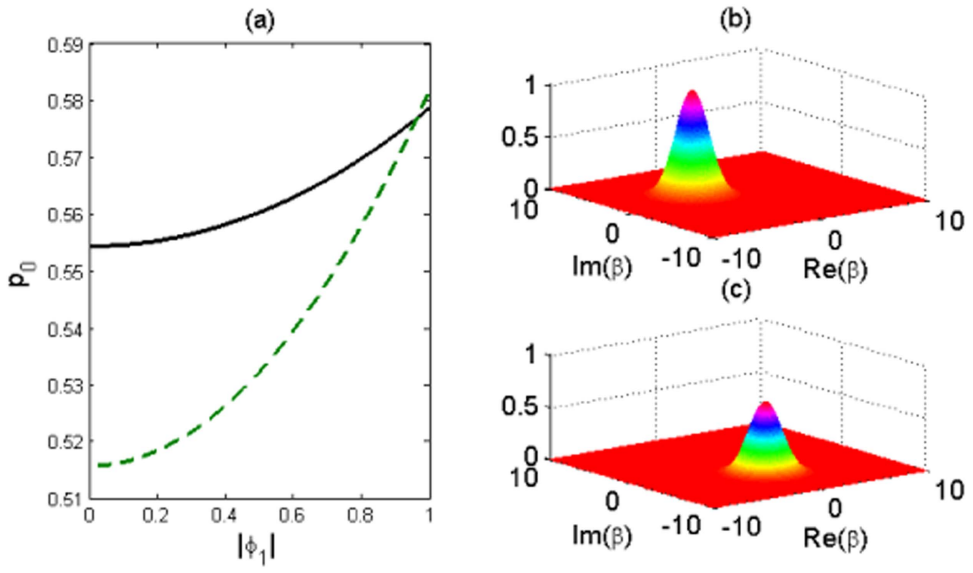

Figure 2. The zero-click probability distribution as a function of the overlap ϕ. The panel (a) shows the dependence of the zero-click probability p_0 on the modulus of the overlap for the signal in a coherent state (solid line) and a single-photon state (dashed line). The probe is a coherent state with the modulus of the amplitude equal to unity and a random phase. The panels (b), (c) show the zero-click probability for a fixed coherent signal and varied probe, β, for the two different values of the overlap. The panel (b) corresponds to the intensity overlap equal to 1 and the overlap phase of $3\pi/2$ with respect to the phase between the signal and the probe fields; the amplitude of the signal is 2. The panel (c) is for the overlap equal to 0.95. For all the graphs the detection efficiency, $\eta = 0.59$; and the transmittivity of BS, $T^2 = 0.466$; the amplitude of the signal for panels (b), (c) is $2/\sqrt{\eta}T$.

2.2. Inferring the temporal/spectral mode profile

For the set of known overlap values, it is straightforward to infer the product of spectral envelopes of the signal and probe modes. If we vary the overlap using the time-delay for one of the pulses, the product of the frequency profiles of the modes of the signal state, $f_s(\omega)$, and the probe state, $f_p(\omega)$, is connected to the overlap by the Fourier transform:

$$\phi(\delta t) = \int \mathrm{d}\omega f_s(\omega) f_p^*(\omega) \exp\{-\mathrm{i}\omega\delta t\}, \tag{9}$$

where δt is the value of time-delay. The problem of the profile inference remains feasible even in the case of when only the modulus of the overlap is estimated. It is a particular case of much discussed phase-retrieval problem commonly encountered in the image reconstruction (see, for example, the recent brief review [26]). One of the simplest ways to do the profile inference is to represent $f_s(\omega)f_p^*(\omega)$ as a superposition of some localized basis functions, typically the Hermite-Gaussian functions are used. Such a representation is useful, for example, for the reconstruction of the states generated in a spontaneous down conversion schemes [27].

2.3. Inferring the signal state

Finally, let us consider an inference of the signal state by variation of the overlap. Equation (6) can be re-written in the following form

$$p = \frac{\exp\{-(1-T^2)\eta|\beta|^2(1-|\phi_1|^2)\}}{1-\eta T^2} \int \mathrm{d}^2\alpha\ \mathrm{e}^{-\sigma|\alpha-\bar{\beta}|^2} Q(\alpha, \alpha^*), \tag{10}$$

where $\sigma = \frac{\eta T^2}{1-\eta T^2}$, and $Q(\alpha, \alpha^*)$ is the Husimi Q-function for the original signal state ρ_s. Equation (10) is a generalization for the imperfect overlap of the result obtained in [3] for the ideal overlap and guarantees the possibility of the reconstruction by varying the overlap. Indeed, equation (10) is just the the Weierstrass transform which can be inverted (see appendix A). However, to infer a set of discrete parameters, such as density matrix coefficients in the Fock states basis, it is not necessary to revert to the inverse Weierstrass transform. To that end, let us consider representation of ρ_s in some discrete basis. For example, in Fock-state basis the Q-function can be represented as

$$Q(\alpha, \alpha^*) = \frac{1}{\pi}\mathrm{e}^{-|\alpha|^2} \sum_{n,m\geqslant 0} \rho_{n,m} \frac{(\alpha^*)^n \alpha^m}{\sqrt{n!m!}}, \tag{11}$$

where the matrix elements $\rho_{n,m} \equiv \langle n|\rho_s|m\rangle$. From equations (10), (11) it follows that the probability of zero clicks as a function of parameter $\bar{\beta}$ is given by:

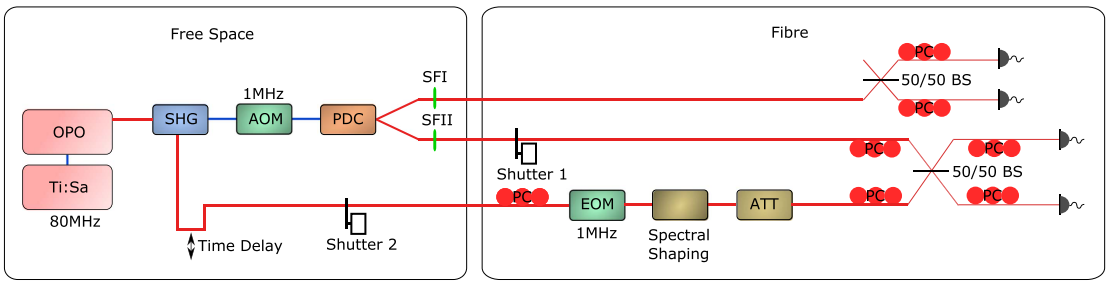

Figure 3. Schematic picture showing the experimental setup. SF: spectral filter; EOM: electro-optic modulator; AOM: acousto-optic modulator; Att: attenuator; PC: polarization controller.

$$p(\bar{\beta}, \bar{\beta}^*) = \exp\{-\eta(1 - T^2)|\beta|^2\}\mathcal{P}(\bar{\beta}, \bar{\beta}^*), \tag{12}$$

where $\mathcal{P}(\bar{\beta}, \bar{\beta}^*)$ is an expansion in *non-negative powers* of $\bar{\beta}$ and $\bar{\beta}^*$, which reads

$$\mathcal{P}(\bar{\beta}, \bar{\beta}^*) = \sum_{n,m\geqslant 0} \frac{\rho_{n,m}}{\sqrt{n!m!}} \exp\left(-\frac{|y|^2}{1+\sigma}\right)\partial_y^n \partial_{y^*}^m \exp\left(\frac{|y|^2}{1+\sigma}\right)\Bigg|_{y=\sigma\bar{\beta}}. \tag{13}$$

Equation (12) points to some important conclusions. First of all, for the realistic finite reconstruction subspace (corresponding to the truncation of the Fock state expansion of the signal density matrix), one can indeed infer the signal state for a finite number of $\bar{\beta}$ values. It is always possible to choose such a number of $\bar{\beta}$ values as to interpolate a continuous function $\mathcal{P}(\bar{\beta}, \bar{\beta}^*)$ by the Lagrange polynomials with sufficient accuracy. This allows then to infer the Q-function. Of course, it is more practical to infer a discrete set of expansion coefficients, $\rho_{m,n}$. This can be done in a number of already well-established ways (for example, by inverting equation (5) using constrained least-square methods [22, 23], or maximum-likelihood methods [9]). From equation (5) it also follows that one can get the set of $\bar{\beta}$-points sufficient for reconstruction of any finite-subspace expansion of ρ_s for an arbitrarily small probe state amplitude, β.

To realize the scheme in practice, it is necessary to devise a way to change the overlap to produce the set of values, $\{\bar{\beta}_j\}$, sufficient for the inference. This can be achieved by shaping the spectral profile of the mode (see, for example, [11–18]). However, one really does not need to manipulate precisely a shape of the probe pulse to obtain the necessary set; a simple time-delay arrangement is sufficient (see section 3 for details).

In conclusion of this section, it is instructive to outline a difference between a reconstruction by varying the amplitude of the probe field and the overlap. Equation (6) seems to suggest that both methods are similar. However, in fact they are not. The difference can be well illustrated with just coherent signal and probe states. It is easy to see that the logarithm of the zero click probability,

$$\ln p = -T^2\eta(|\alpha|^2 + \mu^2|\beta|^2 + \mu\phi_1\alpha^*\beta + \mu\phi_1^*\beta^*\alpha)$$

is a quadratic function of the probe field amplitude, β (and the signal field amplitude, α). But $\ln p$ is a linear function of the overlap value. Thus, without knowledge of the signal state, α, it is not possible to reproduce a set of probabilities obtained by the variation of the overlap with the set of probabilities obtained by variation of the probe state amplitude (even up to some constant multiplier). Also, obviously, informational content of both measurements is quite different (see the appendix B for the Fisher information calculation).

3. Experimental results

We illustrate the possibility of the single-mode state-profile trade-off with single and two-photon states obtained using the usual parametric down-conversion scheme. The setup used for this experiment is shown in figure 3. The signal is generated in an engineered periodically poled potassium titanyl phosphate (KTP) waveguide (AdvR) with a type-II parametric down-conversion process [28]. The source can generate a nearly spectrally decorrelated state at 1550 nm. The down conversion is pumped at 775 nm with frequency doubled light from an OPO system (Coherent Chameleon Compact OPO). The residual pump light from the OPO at 1550 nm is used as a weak probe field. To adapt the spectrum of the probe field to the signal, spectral shaping involving bandwidth and spectral phase (Finisar Waveshaper 4000) is employed. An automated free space variable delay line is used to change the relative timing between signal and probe. Both fields are then combined on a fiber integrated BS. The idler mode from the parametric down conversion is split on a second 50/50 BS allowing for heralding on one or two clicks. The light is detected with superconducting nano-wire detectors (Photon Spot). The repetition rate of the experiment is limited to 1 MHz. An acousto-optic modulator is used to lower the repetition rate for the 775 nm light whereas a fiber integrated electro-optic modulator is used for the probe field.

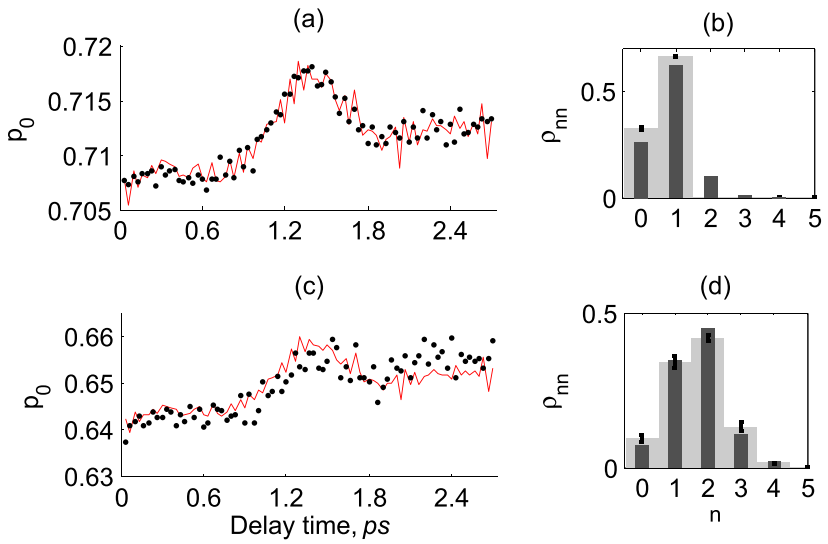

Figure 4. Experimental results for the quantum state reconstruction of the single-mode signal and probe. (a) Zero-click probability for the single-photon state. Black points correspond to the measured data; red line corresponds to the fit. (b) The inferred photon-number distribution for the single-photon state (wide light-gray bars). Narrow dark-gray bars correspond to the state estimate obtained for the fixed detector efficiency and known parameters of the signal. (c) Zero-click probability for the two-photon state. Black points correspond to the measured data; red line corresponds to the fit. Different values of the overlap were obtained by delaying the probe pulse. (d) The inferred photon-number distribution for the two-photon state. Narrow dark-gray bars correspond to the state estimate obtained for the fixed detector efficiency and known parameters of the signal. Higher photon number components arise from the strongly pump down-conversion in combination with loss during the heralding process. For all the graphs the efficiency, $\eta = 0.59$; $|U_{1,2}|^2 = 0.544$; $U_{1,2}$ and $U_{1,1}$ are taken to be real.

A total of 81 different delays between signal and probe where scanned with an acquisition time of 150 s each. Between these measurements automated shutters were used to either measure the PDC signal or the probe field to account for long term drifts. While only using the PDC signal (shutter 2 is closed) the Klyshko efficiency can be measured giving the product of all efficiencies after the PDC [29]. In addition a calibrated coherent state is used to measure the efficiency from the BS (where signal and probe are combined) to the detectors. The BS has a slight asymmetry with a transmittivity of 43.6. The overlap is estimated by analyzing the Hong–Ou–Mandel interference pattern between probe and signal. The multi-photon components in the signal and probe reduced the visibility of the Hong–Ou–Mandel interference, even in the case of perfect modal overlap. The probe field with the average number of photons 0.19 was used.

The results of the quantum state reconstruction for the single-photon and two-photon states are displayed in figures 4(b), (d). Estimation of the photon-number distributions was performed using equations (5), (8) for least squares fit with linear constraints[5]. Notice that the registered experimental data (figures 4(a), (c)) show presence of significant efficiency drifts due to rather long acquisition time and temperature instabilities. These drifts were estimated by measuring the zero-click probability in the absence of the probe and incorporated in the model. Initial efficiency of the detector including all losses after the BS was found to be $\eta = 0.59$. This efficiency was measured using a known birght coherent state and calibrated attenuators. In figures 4(b), (d) we have also shown single and two-photon states estimated from known parameters of the state generated by the parametric down conversion (narrow dark-gray bars). They are obtained for the squeezing value of $r = 0.382$ and fixed efficiency η. Notably, one can see despite the drifts, the two-photon states obtained by different estimation methods are quite close.

The crucial part of the procedure is the experimental inference of the actual value of the overlap as was described in section 2.1. The overlap profile inferred for the single-photon states is shown in figure 5.

Here one should emphasize the different role played by the overlap in different measurement schemes, in particular, in homodyning with a strong probe and non-balanced scheme with the weak probe as the one described and implemented in our work. In balanced homodyning with a strong probe the role of the finite overlap is equivalent to additional detection loss. As it was shown in the section 2.3 and appendix B, the role of the overlap for the non-balanced scheme with a weak probe is quite different. The phase of the overlap is rather important for the complete reconstruction (this one can see, for example, in figure 2(b)). As we have demonstrated here, it is possible to build a set of measurements sufficient for the complete reconstruction of the signal by varying the phase and the modulus of the overlap for the fixed coherent probe. Finally, with the weak

[5] Error estimation was performed for 100 sets of the input data generated by randomly taking out one value from 15 of those corresponding to each overlap value and summing the rest; for each set the second bootstrap was performed taking 1000 random sets of 81 overlap points.

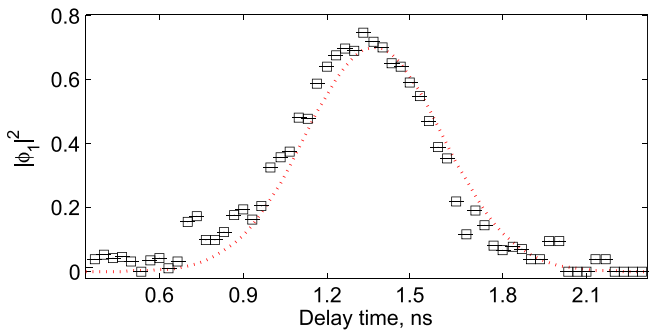

Figure 5. Experimental results for the overlap inference for the coherent probe and the single-photon signal. Dotted red line shows the provided overlap values; squares shows the inferred overlap values for the inferred single photon state, $0.335|0\rangle\langle 0| + 0.665|1\rangle\langle 1|$. Other parameters are as for figure 4.

probe one can infer the modulus of the overlap even without knowing the signal [9] by additional variation of the detector efficiency. So, the weak-probe scheme indeed gives the possibility to detect appearance of distinguishability between the signal and probe modes.

4. Scheme for the multi-mode fields

Finally, let us show how the state of an arbitrary multi-mode field can be inferred with the simplest measurement set-up with on/off detectors. The signal field is mixed with the probe field on the BS; the outputs (or just one of them) are impinging on the on/off detectors as depicted in figure 1(B).

As illustrated in figure 1(B), the imperfect overlap on the BS can be modeled by separating the input fields into the modes perfectly overlapping on the BS ('modes mixed by BS') and the modes with zero overlap thus not interacting on the BS ('modes not mixed by BS'). Then let the two inputs and two outputs on a BS be given by the mode creation operators $a^\dagger_{k,s}$ and $b^\dagger_{k,s}$, where $k = 1, 2$ is the operating mode mixed by the BS (solid red lines in figure 1(B)), whereas $s = 1, \ldots, S$ enumerates the basis of the invariant modes, i.e., not mixed by the BS (various dashed and dashed–dotted lines in figure 1(B)). The BS itself is represented by a unitary matrix U which relate the output to the input operators:

$$b^\dagger_{k,s} = \sum_{l=1,2} U_{k,l} a^\dagger_{l,s}. \tag{14}$$

In the matrix form it can be written as $\mathbf{b}^\dagger = (U \otimes I)\mathbf{a}^\dagger$, where I is the S-dimensional identity matrix and $\mathbf{a} = (\mathbf{a}_1, \mathbf{a}_2)$ with $\mathbf{a}_k = (a_{k,1}, \ldots, a_{k,S})$, etc.

Consider an arbitrary multi-mode state at input k and the non-ideal on–off type detector placed at the outputs of the BS. The quantum state $\rho^{(k)}$ of the input modes k can be conveniently written in Fock basis as

$$\rho^{(k)} = \sum_{\mathbf{n},\mathbf{m}\geqslant 0} \rho^{(k)}_{\mathbf{n},\mathbf{m}} |\mathbf{n}\rangle\langle\mathbf{m}|, \qquad |\mathbf{n}\rangle \equiv \prod_{s=1}^{S} \frac{(a^\dagger_{ks})^{n_s}}{\sqrt{n_s!}}|0\rangle. \tag{15}$$

Note that in this expression the multi-mode character of the field is encapsulated in quantities in bold, e. g., $|\mathbf{n}\rangle$ and $\mathbf{n} \equiv (n_1, \ldots, n_S)$. Let η_k be the sensitivity of the detector at output mode $k = 1, 2$. We are interested in the probability that the detector k does not click. Such probabilities of no clicks at the outputs (zero-click probabilities) are given by the generating function:

$$\begin{aligned} P(\eta_1, \eta_2) &\equiv \mathrm{Tr}\left(\rho^{(1)} \otimes \rho^{(2)} \mathcal{N}\exp\left[-\sum_{k=1,2} \eta_k \sum_{s=1}^{S} b^\dagger_{k,s} b_{k,s}\right]\right) = \mathrm{Tr}\left(\rho^{(1)} \otimes \rho^{(2)} \mathcal{N}\exp\left\{-\mathbf{b}\left[\begin{pmatrix}\eta_1 & 0\\ 0 & \eta_2\end{pmatrix} \otimes I\right]\mathbf{b}^\dagger\right\}\right) \\ &= \mathrm{Tr}\left(\rho^{(1)} \otimes \rho^{(2)} \mathcal{N}\exp\left\{-\mathbf{a}\left[U^\dagger\begin{pmatrix}\eta_1 & 0\\ 0 & \eta_2\end{pmatrix} U \otimes I\right]\mathbf{a}^\dagger\right\}\right), \end{aligned} \tag{16}$$

where $\mathcal{N}$ denotes the normal ordering of the creation and annihilation operators. For example, to calculate the probability of no clicks at detector 1, $p_1(\eta_1)$, we set $\eta_2 = 0$ in equation (16), that is $p_1(\eta_1) = P(\eta_1, 0)$.

To compute the probabilities from the family of $P(\eta_1, \eta_2)$ in equation (16), we use the following identity

$$\mathcal{N}\exp\{-\mathbf{a}(I - H)\mathbf{a}^\dagger\} = \frac{\mathcal{A}\exp\{-\mathbf{a}(H^{-1} - I)\mathbf{a}^\dagger\}}{\det(H)}, \tag{17}$$

where $\mathcal{A}$ denotes the antinormal ordering of the creation and annihilation operators and H is some positive semi-definite Hermitian matrix with eigenvalues bounded by 1. Equation (17) can be verified by diagonalizing the matrix H, performing the series expansion of the exponents and checking the equality of both sides using the Fock states. In equation (16) we can identify the matrix H and find its inverse as:

$$H = U^{\dagger}\begin{pmatrix} 1-\eta_1 & 0 \\ 0 & 1-\eta_2 \end{pmatrix} U \otimes I, \quad H^{-1} = A \otimes I, \quad A \equiv U^{\dagger}\begin{pmatrix} \frac{1}{1-\eta_1} & 0 \\ 0 & \frac{1}{1-\eta_2} \end{pmatrix} U. \tag{18}$$

Note also that $\det(H) = (1-\eta_1)^S(1-\eta_2)^S$. Substituting equations (17) and (18) into equation (16) we then obtain:

$$P(\eta_1, \eta_2) = \frac{1}{(1-\eta_1)^S(1-\eta_2)^S}\,\mathrm{Tr}\,(\rho^{(1)} \otimes \rho^{(2)}\mathcal{A}\exp\{-\mathbf{a}([A-I]\otimes I)\mathbf{a}^{\dagger}\}). \tag{19}$$

We can evaluate the trace in equation (19) in the coherent state basis $|\boldsymbol{\alpha}_k\rangle \equiv |\alpha_{k,1}\rangle \otimes \ldots \otimes |\alpha_{k,S}\rangle$ by introducing the generalized (multimode) Husimi function for each input state,

$$Q^{(k)}(\boldsymbol{\alpha}, \boldsymbol{\alpha}^{\dagger}) \equiv \frac{1}{\pi^S}\langle\boldsymbol{\alpha}|\rho^{(k)}|\boldsymbol{\alpha}\rangle. \tag{20}$$

The generalized Hiusimi function is normalized, $\int \mathrm{d}\mu(\boldsymbol{\alpha})Q^{(k)}(\boldsymbol{\alpha}, \boldsymbol{\alpha}^{\dagger}) = 1$ where $\mathrm{d}\mu(\boldsymbol{\alpha}) \equiv \prod_{s=1}^{S} \mathrm{d}^2\alpha_s$ with $\mathrm{d}^2\alpha_s = \mathrm{d}\mathrm{Re}\alpha_s\,\mathrm{d}\,\mathrm{Im}\,\alpha_s$ and $\boldsymbol{\alpha} = (\boldsymbol{\alpha}_1, \ldots, \boldsymbol{\alpha}_S)$. From equations (19) and (20) we obtain

$$P(\eta_1, \eta_2) = \int \mathrm{d}\mu(\boldsymbol{\alpha}_1)\int \mathrm{d}\mu(\boldsymbol{\alpha}_2)Q^{(1)}(\boldsymbol{\alpha}_1, \boldsymbol{\alpha}_1^{\dagger})Q^{(2)}(\boldsymbol{\alpha}_2, \boldsymbol{\alpha}_2^{\dagger})\frac{\exp\{-\vec{\boldsymbol{\alpha}}([A-I]\otimes I)\vec{\boldsymbol{\alpha}}^{\dagger}\}}{(1-\eta_1)^S(1-\eta_2)^S}. \tag{21}$$

Here we have introduced the combined vector variable $\vec{\boldsymbol{\alpha}} \equiv (\boldsymbol{\alpha}_1, \boldsymbol{\alpha}_2)$ with $\boldsymbol{\alpha}_k = (\alpha_{k,1}, \ldots, \alpha_{k,S})$. The probabilities of no click given by equation (21) provide the key relation for the reconstruction of an arbitrary multimode field in quantum state $\rho^{(1)}$ by mixing it with a probe field $\rho^{(2)}$ on a BS with the use of the non-ideal on–off type detector(s).

For a set of coherent probes available in different modes the scheme becomes particularly simple. It allows us to infer the multi-mode signal collecting a string of zeros and ones on merely one on/off detector. Let $\rho^{(2)} = |\boldsymbol{\beta}\rangle\langle\boldsymbol{\beta}|$ for some $\boldsymbol{\beta} = (\boldsymbol{\beta}_1, \ldots, \boldsymbol{\beta}_S)$. We have

$$Q^{(2)}(\boldsymbol{\alpha}_2, \boldsymbol{\alpha}_2^{\dagger}) = \frac{1}{\pi^S}\exp\{-|\boldsymbol{\alpha}_2 - \boldsymbol{\beta}|^2\}. \tag{22}$$

To derive the expression for the probabilities, we use the identities for the BS transformation matrices: $|U_{k1}|^2 + |U_{k2}|^2 = 1$, $U_{11}U_{21}^* = -U_{12}U_{22}^*$, $|U_{11}| = |U_{22}|$, and $|U_{12}| = |U_{21}|$, which result from the unitarity of the two-dimensional matrix U of the BS. For the Gaussian integrals, the following standard relation holds:

$$\int \frac{\mathrm{d}\mu(\boldsymbol{\alpha})}{\pi^S}\exp\{-\boldsymbol{\alpha}B\boldsymbol{\alpha}^{\dagger} + \boldsymbol{\alpha}\mathbf{h}^{\dagger} + \mathbf{g}\boldsymbol{\alpha}^{\dagger}\} = \frac{\exp\{\mathbf{g}B^{-1}\mathbf{h}^{\dagger}\}}{\det(B)}, \tag{23}$$

where $\boldsymbol{\alpha} = (\alpha_1, \ldots, \alpha_S)$, B is a positive semi-definite Hermitian matrix, while $\mathbf{g}$ and $\mathbf{h}$ are S-dimensional vector rows. Substituting (22) into (21) and evaluating the Gaussian integral over $\boldsymbol{\alpha}_2$ using equation (23), we obtain

$$P(\eta_1, \eta_2) = \varkappa^{-S}\exp\left\{-\frac{\eta_1\eta_2}{1-\varkappa}|\boldsymbol{\beta}|^2\right\}\int \mathrm{d}\mu(\boldsymbol{\alpha})\exp\left\{-\frac{1-\varkappa}{\varkappa}\left|\boldsymbol{\alpha} + \frac{(\eta_1-\eta_2)U_{11}U_{21}^*}{1-\varkappa}\boldsymbol{\beta}\right|^2\right\}Q^{(1)}(\boldsymbol{\alpha}, \boldsymbol{\alpha}^{\dagger}), \tag{24}$$

where $\varkappa = 1 - \eta_1|U_{11}|^2 - \eta_2|U_{21}|^2$.

Now, notably, for the coherent probes $\rho^{(2)} = |\boldsymbol{\beta}\rangle\langle\boldsymbol{\beta}|$, the reconstruction of the multi-mode source field $\rho^{(1)}$ is possible from the no clicks probability even on just one detector, $P(\eta_1, 0)$, setting $\eta_2 = 0$ in equation (24). This is due to the fact that the expression in equation (24) is proportional to a multidimensional Weierstrass transform of the Husimi function of the source field, which allows for the inverse transform by the properties of the Husimi function (see appendix).

5. Conclusions

Here we have shown that the state of an arbitrary multi-mode field can be inferred using the imperfect overlap between the signal and the reference fields using just one on/off detector. Moreover, information about the temporal structure of the field can be traded for the information about the quantum state of this field, and vice versa and reconstruction of both can be realized with the same measurement set-up. The key for such a measurement scheme is to vary the imperfect mode overlap in a controlled way.

For the single mode signal and reference fields, we show experimentally that this can be achieved by the simple time delay of the probe. An important step in the procedure is the experimental estimation of the actual value of the mode overlap ϕ_1 (2). Remarkably, for the single-mode case and for probe or signal in a diagonal state, for the known signal the overlap can be inferred with just one fixed probe state. The experimental results for the quantum state inference from the knowledge of the spectral profile by changing the overlap, and the reverse problem of estimating the overlap from the knowledge of the signal state, are depicted in figure 5. The suggested scheme can be used for diagnostics of devices (such as quantum pulse gate) which can possibly alter both temporal profile and quantum states of the field.

Thus we have shown that the distinguishability of modes can be a valuable resource. It can be implemented for quantum state diagnostics and tomography. Actually, distinguishability and imperfect overlap of the probe and signal is a bridge which allows to connect spacial, temporal and spectral features of wave-package carrying the quantum state and parameters of this state.

Acknowledgments

VS acknowledge support from the National Council for Scientific and Technological Development (CNPq) of Brazil, grant 304129/2015-1, and by the São Paulo Research Foundation (FAPESP), grant 2015/23296-8. DM acknowledge support from the EU project Horizon-2020 SUPERTWIN id.686731, the National Academy of Sciences of Belarus program 'Convergence' and FAPESP grant 2014/21188-0. NK acknowledges the support from the Scottish Universities Physics Alliance (SUPA) and from the International Max Planck Partnership (IMPP) with Scottish Universities. JT and CS acknowledge support from European Union Grant No. 665148 (QCUMbER). TB acknowledges support from the DFG under TRR 142.

Appendix A

The multidimensional Weierstrass transform of a function $Q(\boldsymbol{\alpha})$ of a complex variable $\boldsymbol{\alpha} = (\alpha_1, \ldots, \alpha_S) \in C^S$ is defined as a convolution with the following multidimensional Gaussian (for $\sigma > 0$)

$$\mathcal{W}(\boldsymbol{\alpha}, \boldsymbol{\alpha}^\dagger) = \int \mathrm{d}\mu(\boldsymbol{\beta}) \mathrm{e}^{-\sigma|\boldsymbol{\alpha}-\boldsymbol{\beta}|^2} Q(\boldsymbol{\beta}, \boldsymbol{\beta}^\dagger), \tag{25}$$

where $\boldsymbol{\beta} = (\beta_1, \ldots, \beta_S) \in C^S$. Assuming that there is the (multidimensional) Fourier transform of $Q(\boldsymbol{\alpha})$ (as in the case of the Husimi function equation (20)), one can show that there is the inverse transform to equation (25). Let us write the Fourier transform using the complex variables:

$$Q(\boldsymbol{\alpha}, \boldsymbol{\alpha}^\dagger) = \int \frac{\mathrm{d}\mu(\mathbf{z})}{\pi^S} \exp\{\mathbf{z}\boldsymbol{\alpha}^\dagger - \boldsymbol{\alpha}\mathbf{z}^\dagger\} F(\mathbf{z}, \mathbf{z}^\dagger), \quad F(\mathbf{z}, \mathbf{z}^\dagger) = \int \frac{\mathrm{d}\mu(\boldsymbol{\alpha})}{\pi^S} \exp\{\boldsymbol{\alpha}\mathbf{z}^\dagger - \mathbf{z}\boldsymbol{\alpha}^\dagger\} Q(\boldsymbol{\alpha}, \boldsymbol{\alpha}^\dagger). \tag{26}$$

Substituting the Fourier transform of equation (26) into equation (25) and evaluating the Gaussian integral with the help of equation (23), we can put the Weierstrass transform in the differential operator form (i.e., an infinite series expansion):

$$\mathcal{W}(\boldsymbol{\alpha}, \boldsymbol{\alpha}^\dagger) = \left(\frac{1}{\sigma}\right)^S \int \mathrm{d}\mu(\mathbf{z}) \exp\left\{\mathbf{z}\boldsymbol{\alpha}^\dagger - \boldsymbol{\alpha}\mathbf{z}^\dagger - \frac{|\mathbf{z}|^2}{\sigma}\right\} F(\mathbf{z}, \mathbf{z}^\dagger) = \left(\frac{\pi}{\sigma}\right)^S \exp\left\{\frac{1}{\sigma}\sum_{s=1}^{S} \frac{\partial^2}{\partial\alpha_s^* \partial\alpha_s}\right\} Q(\boldsymbol{\alpha}, \boldsymbol{\alpha}^\dagger). \tag{27}$$

Equation (27) has the inverse transformation (in the form of an infinite series)

$$Q(\boldsymbol{\alpha}, \boldsymbol{\alpha}^\dagger) = \left(\frac{\sigma}{\pi}\right)^S \exp\left\{-\frac{1}{\sigma}\sum_{s=1}^{S} \frac{\partial^2}{\partial\alpha_s^* \partial\alpha_s}\right\} \mathcal{W}(\boldsymbol{\alpha}, \boldsymbol{\alpha}^\dagger). \tag{28}$$

The infinite series representation of equation (28) for the Husimi function from its Weierstrass transform can be recast in the explicit form as an integral in R^{2S}. Substituting the operator identity

$$\exp\left\{-\frac{1}{\sigma}\sum_{s=1}^{S} \frac{\partial^2}{\partial\alpha_s^* \partial\alpha_s}\right\} = \left(\frac{\sigma}{\pi}\right)^S \int \mathrm{d}\mu(\mathbf{z}) \exp\left\{-\sigma|\mathbf{z}|^2 + \mathrm{i}\left(\sum_{s=1}^{S} z_s^* \frac{\partial}{\partial\alpha_s} + z_s \frac{\partial}{\partial\alpha_s^*}\right)\right\} \tag{29}$$

(derived by using equation (23)) into equation (28) and setting $z_s = x_s + \mathrm{i}y_s$, we obtain:

$$\begin{aligned} Q(\boldsymbol{\alpha}, \boldsymbol{\alpha}^\dagger) &= \left(\frac{\sigma}{\pi}\right)^{2S} \int \mathrm{d}\mu(\mathbf{z}) \exp\left\{-\sigma|\mathbf{z}|^2 + \mathrm{i}\left(\sum_{s=1}^{S} x_s \frac{\partial}{\partial \operatorname{Re}\alpha_s} + y_s \frac{\partial}{\partial \operatorname{Im}\alpha_s}\right)\right\} \mathcal{W}(\boldsymbol{\alpha}, \boldsymbol{\alpha}^\dagger) \\ &= \left(\frac{\sigma}{\pi}\right)^{2S} \int \prod_{s=1}^{S} \mathrm{d}x_s \mathrm{d}y_s \exp\left\{-\sigma\sum_{s=1}^{S}(x_s^2 + y_s^2)\right\} \mathcal{W}_R(\operatorname{Re}\boldsymbol{\alpha} + \mathrm{i}\mathbf{x}, \operatorname{Im}\boldsymbol{\alpha} + \mathrm{i}\mathbf{y}), \end{aligned} \tag{30}$$

where $\mathcal{W}_R(\operatorname{Re}\boldsymbol{\alpha}, \operatorname{Im}\boldsymbol{\alpha})$ is the Weierstrass transform $\mathcal{W}(\boldsymbol{\alpha}, \boldsymbol{\alpha}^\dagger)$ expressed as a function of the real and imaginary parts of the complex vectorα.

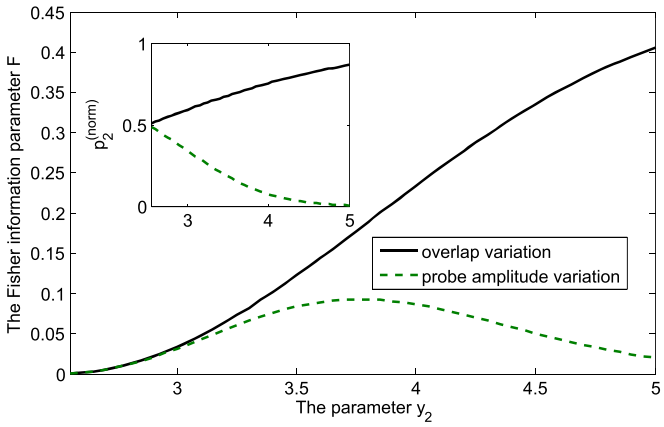

Figure B1. An example of the Fisher information parameter for the schemes of the overlap variation (black solid line) and the probe amplitude variation (green dashed line). The Fisher information parameter is given by the variation of the second measurement point defined by $y_2 = \beta_2 = \phi_2\beta_0$. The inset shows the normalized probabilities $p_2^{\mathrm{norm}} = p_2/(p_1 + p_2)$, where p_j are given by equations (31), (32). The first measurement is made for $\beta_1 = 0.5\beta_0$, or for $\phi = 0.5$. For all calculations here we have $\beta_0 = 5, \alpha = 1, \eta = 0.75$.

Appendix B

Let us consider the basic example of a coherent signal and coherent probe. For the sake of simplicity, we assume real amplitudes and overlaps, and a 50/50 BS for the on/off detection scheme with detector efficiency η. The first measurement scheme that we consider is to vary the probe amplitude and measure the frequencies of 'no-clicks' for the unit overlap. For this scheme, the probabilities are given by the following formula (we chose the detection scheme to give us vacuum on the output of the BS for the probe and signal with equal amplitudes)

$$p_j^a = \exp\{-0.5\eta(\alpha^2 + \beta_j^2 - 2\alpha\beta_j)\}. \tag{31}$$

For this scheme we assume $\beta \in [0,\ \beta_0]$.

Next, we consider the scheme with variation of the overlap for the coherent signal and the coherent probe with the fixed amplitude β_0. In this case, the probability of 'no-clicks' is given by the following expression [4]:

$$p_j^o = \exp\{-0.5\eta(\alpha^2 + \beta_0^2 - 2\phi_j\alpha\beta_0)\} = \exp\{-0.5\eta(\alpha - \phi_j\beta_0)^2 - 0.5\eta\beta_0^2(1 - \phi_j^2)\}, \tag{32}$$

where ϕ_j is the overlap.

Now let us try to choose a sequence of the overlap values, which reproduce the probabilities obtained by the variation of the probe up to some constant multiplier ('background'). So, we seek

$$p_j^o = p_j^a \exp\{-0.5\eta x\}, \tag{33}$$

where the parameter x does not depend on ϕ_j or β_j. From equation (33) we have

$$\phi_j = \frac{\beta_j}{\beta_0} - \frac{x + \beta_j^2 - \beta_0^2}{2\alpha\beta_0}. \tag{34}$$

Obviously, without knowing *a priori* the amplitude α, it is not possible to choose the set of β_j to achieve the same set of probabilities p_j, up to some constant background.

Now let us demonstrate an example of the scheme giving an information advantage to the overlap variation procedure. We specify some maximal probe amplitude, β_0. We aim to infer the unknown signal amplitude. We take just two such measurements with the overlap variation scheme, and just two measurements with the probe variation scheme assuming that $\beta_j = \phi_j\beta_0$. The informational content can be characterized by the Fisher information parameter

$$F = \sum_{\forall j} \frac{p_j}{P}\left[\frac{\partial}{\partial\alpha}\ln\frac{p_j}{P}\right]^2 = \frac{1}{P}\left(\sum_{\forall j}\frac{1}{p_j}\left[\frac{\partial p_j}{\partial\alpha}\right]^2 - \frac{1}{P}\left[\frac{\partial P}{\partial\alpha}\right]^2\right), \tag{35}$$

where $P = \sum_{\forall j} p_j$, and the probabilities are given by equations (31), (32). The Fisher information parameter gives a lower bound of the variance of the signal amplitude unbiased estimation via the Cramer–Rao inequality, $\Delta_\alpha^2 \geqslant [FN]^{-1}$. For this case, N is the total number of 'no-clicks' for both measurements.

An example of the Fisher information calculation can be seen in figure B1. We keep the parameter $y_2 = \beta_2 = \phi_2\beta_0$ equal for both schemes. The first measurement is taken in the middle of the interval ($\beta_1 = 0.5\beta_0$, or $\phi_1 = 0.5$), the second is varied through the second half of the interval. The amplitude of the signal is $\alpha = 1$ in the first half of the interval.

One can see from figure B1 that in our simple scheme, varying the overlap gives a better lower bound on estimation errors (higher Fisher information) than varying the probe state amplitude.

ORCID iDs

V S Shchesnovich https://orcid.org/0000-0002-6294-4993
V Ansari https://orcid.org/0000-0002-4020-0627
Ch Silberhorn https://orcid.org/0000-0002-2349-5443

References

[1] Vogel K and Risken H 1989 *Phys. Rev.* A **40** 2847(R)
[2] Paris M G A and Řeháček J (ed) 2004 *Quantum States Estimation* (*Lecture Notes in Physics* vol 649) (Berlin: Springer) (https://doi.org/10.1007/b98673)
[3] Wallentowitz S and Vogel W 1996 *Phys. Rev.* A **53** 4528
[4] Laiho K, Cassemiro K N, Gross D and Silberhorn C 2010 *Phys. Rev. Lett.* **105** 253603
[5] Mogilevtsev D 1998 *Opt. Commun.* **156** 307
Mogilevtsev D 1999 *Acta Phys. Slovaca* **49** 743
[6] Harder G, Mogilevtsev D, Korolkova N and Silberhorn C 2014 *Phys. Rev. Lett.* **113** 070403
[7] Rossi A R, Olivares S and Paris M G A 2004 *Phys. Rev.* A **70** 055801
Rossi A R and Paris M G A 2005 *Eur. Phys. J.* D **32** 223
Zambra G, Andreoni A, Bondani M, Gramegna M, Genovese M, Brida G, Rossi A and Paris M G A 2005 *Phys. Rev. Lett.* **95** 063602
[8] Hradil Z, Mogilevtsev D and Řeháček J 2006 *Phys. Rev. Lett.* **96** 230401
Mogilevtsev D, Řeháček J and Hradil Z 2007 *Phys. Rev.* A **75** 012112
[9] Mogilevtsev D, Rehacek J and Hradil Z 2010 *Phys. Rev.* A **79** 020101(R)
[10] Shchesnovich V S 2014 *Phys. Rev.* A **89** 022333
Shchesnovich V S 2015 *Phys. Rev.* A **91** 013844
[11] Bellini M, Marin F, Viciani S, Zavatta A and Arecchi F T 2003 *Phys. Rev. Lett.* **90** 043602
[12] Pe'er A, Dayan B, Friesem A A and Silberberg Y 2005 *Phys. Rev. Lett.* **94** 073601
[13] Eckstein A, Brecht B and Silberhorn C 2011 *Opt. Express* **19** 13770
[14] Brecht B, Eckstein A, Ricken R, Quiring V, Suche H, Sansoni L and Silberhorn C 2014 *Phys. Rev.* A **90** 030302(R)
[15] Brecht B, Reddy D V, Silberhorn C and Raymer M G 2015 *Phys. Rev.* X **5** 041017
[16] Agha I, Ates S, Sapienza L and Srinivasan K 2014 *Opt. Lett.* **39** 5677
[17] Andrews R W, Reed A P, Cicak K, Teufel J D and Lehnert K W 2015 *Nat. Commun.* **6** 10021
[18] Reddy D V and Raymer M G 2017 *Opt. Express* **25** 12952
[19] Polycarpou C, Cassemiro K N, Venturi G, Zavatta A and Bellini M 2012 *Phys. Rev. Lett.* **109** 053602
[20] Seveso L, Rossi M A C and Paris M G A 2017 *Phys. Rev.* A **95** 012111
[21] Rehacek J, Mogilevtsev D and Hradil Z 2010 *Phys. Rev. Lett.* **105** 010402
[22] Mogilevtsev D, Ignatenko A, Maloshtan A, Stoklasa B, Rehacek J and Hradil Z 2013 *New J. Phys.* **15** 025038
[23] Motka L, Stoklasa B, Rehacek J, Hradil Z, Karasek V, Mogilevtsev D, Harder G, Silberhorn C and Sanchez-Soto L L 2014 *Phys. Rev.* A **89** 054102
[24] Cooper M, Karpinski M and Smith B J 2014 *Nat. Commun.* **5** 4332
[25] Harder G, Silberhorn C, Rehacek J, Hradil Z, Motka L, Stoklasa B and Sanchez-Soto L L 2014 *Phys. Rev.* A **90** 042105
[26] Shechtman Y, Eldar Y C, Cohen O, Chapman H N, Miao J and Segev M 2015 *IEEE Signal Process. Mag.* **32** 87
[27] Ansari V, Allgaier M, Sansoni L, Brecht B, Roslund J, Treps N, Harder G and Silberhorn C 2016 arXiv:1607.03001
[28] Harder G, Ansari V, Brecht B, Dirmeier T, Marquardt C and Silberhorn C 2013 *Opt. Express* **21** 13975–85
[29] Klyshko D 1980 *Quantum Electron.* **10** 1112–7
[30] Dorfman K E, Schlawin F and Mukamel S 2014 *J. Phys. Chem. Lett.* **5** 2843
[31] Brecht B, Eckstein A, Christ A, Suche H and Silberhorn C 2011 *New J. Phys.* **13** 065029
[32] Reddy D V, Raymer M G, McKinstrie C J, Mejling L and Rottwitt K 2013 *Opt. Express* **21** 13840
[33] Manurkar P, Jain N, Silver M, Huang Y-P, Langrock C, Fejer M M, Kumar P and Kanter G S 2016 *Optica* **3** 1300–7
[34] Manurkar P, Jain N, Silver M, Huang Y-P, Langrock C, Fejer M M, Kumar P and Kanter G S 2017 *Opt. Lett.* **42** 951
[35] Valencia A, Cere A, Shi X, Molina-Terriza G and Torres J P 2007 *Phys. Rev. Lett.* **99** 243601